Green Chemistry

PAPER

View Article Online
View Journal | View Issue

Cite this: *Green Chem.*, 2018, **20**, 4085

Heterogenization of homogeneous chiral polymers in metal–organic frameworks with enhanced catalytic performance for asymmetric catalysis†

Xiao-Wu Dong, *[a] Yong Yang,[a,b] Jin-Xin Che,[a] Jun Zuo,[a] Xiao-Hua Li,[c] Liang Gao, [d] Yong-Zhou Hu[a] and Xin-Yuan Liu *[c]

Received 27th April 2018,
Accepted 1st August 2018

DOI: 10.1039/c8gc01323c

rsc.li/greenchem

Metal–organic framework (MOF)-based asymmetric heterogeneous catalysts have attracted increasing attention; however, some challenges need to be addressed, such as the rigidity of chiral auxiliary groups within MOFs and the lack of a versatile methodology for the facile construction of chiral MOFs. To address this issue, in this study, a mechanistically distinct approach was developed for heterogenizing linear chiral catalysts in the MOF cavities, rather than the synthetic modification of MOFs. This strategy involves the facile *in situ* polymerization of pre-impregnated chiral monomers within MOFs, affording the hybrid composites featuring a locally homogeneous and globally heterogeneous structure. The introduced chiral catalytic sites would be flexible in the pores, offering an opportunity to exploit its cooperative effect with the nearby catalytic metal nodes. The advantages of the chiral polymer/MOF composites were clarified by their excellent diastereo- and enantioselectivities and recycling capacity for catalyzing the asymmetric Aldol reaction, which were superior to those of individually heterogeneous and homogeneous catalysts.

Introduction

Biological systems often seamlessly integrate multiple, cooperative functionalities to facilitate specific, highly selective chemical transformations,[1,2] which have been typically revolutionary in artificial catalytic systems, especially for reusable heterogeneous catalysts.[3,4] Nevertheless, some challenges still remain for the design and synthesis of multifunctional heterogeneous catalysts comprising cooperative active sites,[5–8] related to the spatial separation of the active sites within the rigid framework.

As a green and sustainable technology, metal–organic frameworks (MOFs) have been rapidly emerging as an extremely powerful platform for asymmetric catalysts.[9–11] Kim,[12,13] Lin,[14–17] Duan,[18–21] Cui,[22–24] and other research groups[25–28] have successfully reported that a series of homochiral MOFs exhibit catalytic activities for various asymmetric transformations. Generally, the strategies reported for the synthesis of homochiral MOFs are categorized into two groups: (1) direct assembly of compatible chiral organic bridging ligands and metal clusters and (2) introduction of chiral auxiliary groups into the organic linker or unsaturated metal node of achiral MOFs by post-synthetic modifications. With such strategies, all of these introduced catalytic centers were tightly fixed to the wall or metal nodes[29–31] of MOFs with individual compartments separated by a distance, which would limit the cooperative effect between different catalytic sites within MOFs. Thus far, the studies related to the mimicking of biological systems by multi-functionalizing chiral MOFs with cooperative effects are extremely rare. Besides, the nature of a complete heterogeneous catalyst renders it difficult to exactly expose its catalytic sites to substrates in organic reactions because of its limited dissolution in the heterogeneous state.[32,33] Hence, it is of particular importance to develop an attractive alternative functionalization approach for synthesizing chiral MOFs as a green and efficient biomimetic system with the potential for integrating multiple, cooperative functionalities.

To address these challenges, in this study, a mechanistically distinct approach was developed for heterogenizing linear chiral catalysts in the MOF cavities. This strategy was inspired by recent studies of MOF/polymer composites reported by Kitagawa's group,[34,35] in which MOFs can accommodate func-

[a]*Hangzhou Institute of Innovative Medicine, College of Pharmaceutical Sciences, Zhejiang University, Hangzhou, 310058, China. E-mail: dongxw@zju.edu.cn*
[b]*Institute of Pesticide and Environmental Toxicology, Zhejiang University, Hangzhou, 310029, China*
[c]*Department of Chemistry and Shenzhen Grubbs Institute, Southern University of Science and Technology, Shenzhen 518055, China. E-mail: liuxy3@sustc.edu.cn*
[d]*School of Chemical Engineering and Light Industry, Guangdong University of Technology, Guangzhou, 510006, China*

†Electronic supplementary information (ESI) available: Fig. S1–S7, Tables S1–S2, detailed experimental section, NMR spectra, and chiral HPLC spectra. See DOI: 10.1039/c8gc01323c

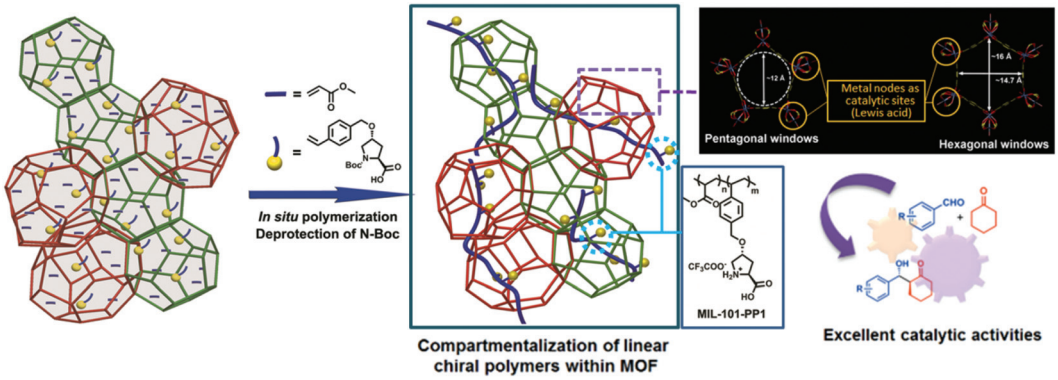

Fig. 1 Schematic diagram for the heterogenization of homogeneous linear chiral catalysts within the cavities of MOFs *via in situ* polymerization to afford chiral polymer/MOF composites, as well as their cooperative effects and excellent catalytic performance in asymmetric Aldol catalysis.

tionalized polymers with practical advantages.[36–42] In principle, although there may exist strong interaction between the pore wall of the MOF and the linear polymer threading throughout the nano-space of MOFs (*e.g.*, hydrophobic interaction and electrostatic interaction), the solvent can significantly reduce net segment–segment forces (*e.g.*, electrostatic and van der Waals force). Therefore, when in contact with appropriate solvents, the polymers in the polymer/MOF composite can detach from the wall of MOFs, but reside in the channel of MOFs due to the confinement effect. Notably, the introduced chiral catalytic sites would be flexible in the pores, offering an opportunity to exploit its cooperative effect with the nearby catalytic metal nodes. In this sense, the composite has the characteristics of a locally homogeneous but globally heterogeneous structure. These features make polymer/MOF composites an ideal support to demonstrate the concept of mimicking of biological catalytic systems by multi-functionalizing chiral MOFs.

Herein, as part of our continued interest in the area of asymmetric catalysis[43–45] and diversely functionalized MOFs,[46–48] we reported novel and reusable highly porous chiral polymer/MOF hybrid composites, which can be used in the asymmetric Aldol reaction. With such strategies, the chiral MOFs could be prepared more readily and economically, since the chiral polymers can be diverse and easily prepared. Moreover, the composites uniquely featuring a heterogeneous matrix and a local homogeneous active domain can exhibit cooperative catalysing capability (Fig. 1). An outstanding performance in catalysing the asymmetric Aldol reaction with good recycling ability was observed, which is much superior to that of conventional chiral MOFs,[13,20,21,23,28] exploiting their respective advantages in the green/sustainable field.[49–52]

Results and discussion

Cr-MIL-101 and L-proline were selected as a pair of cooperative catalysts

Previously, several studies have demonstrated that the combination of Lewis acids and L-proline as the co-catalyst afforded reaction products, with a significantly improved yield and enantioselectivity.[53,54] Thus, in our study, **Cr-MIL-101** was selected as the host material because of its large apparent surface area and uniformly distributed Lewis acid sites,[55,56] and L-proline was used as a model chiral catalyst.[57,58] Indeed, the addition of **Cr-MIL-101** as the co-catalyst, which does not exhibit any catalytic activity (Fig. S1†), can remarkably improve the catalytic performance of L-proline with 75% yield, 86% ee, and 4 : 1 dr, while only an extremely low yield (20%) and poor diastereoselectivity (1.1 : 1) were achieved using 5 mol% of L-proline as the homogeneous catalyst (Fig. S1†).

In situ polymerization of chiral monomers impregnated within Cr-MIL-101

The preparation of the chiral polymer/MOF composites **MIL-101-PP1** is accomplished in two steps *via* an *in situ* polymerization strategy: (1) a solution of the L-proline-containing vinyl derivative S1 (L-proline-containing vinyl monomer, see the ESI† for the details), methyl acrylate and 2,2-azobisisobutyronitrile (AIBN) in toluene is impregnated into the porous cavities of **Cr-MIL-101**; (2) following the incorporation of the monomers, the *in situ* radical copolymerization of the preloaded vinyl compounds was carried out within the MOF framework, affording the polymer/MOF composites **MIL-101-PP1-Boc**. The subsequent deprotection of *N*-Boc groups afforded the desired composite **MIL-101-PP1**. Fig. 2 shows the topological characteristics of **Cr-MIL-101**, the vinyl monomer, and the linear chiral polymer **PP-1**. Their compatible molecular sizes facilitated the complete penetration of the impregnated monomer fluids through the nano-space inside **Cr-MIL-101**. In addition, the amount of the added monomer solution was not greater than the pore volume of **Cr-MIL-101**; thereby most of them were left in the pores. An adequate contact time was required to ensure a thermodynamic equilibrium for the monomer penetration. Next, the monomers were polymerized through windows connecting the different cages of **Cr-MIL-101** and intertwined together.

After polymerization, chiral polymeric chains were immobilized within the ordered mesopores of **Cr-MIL-101**, as shown

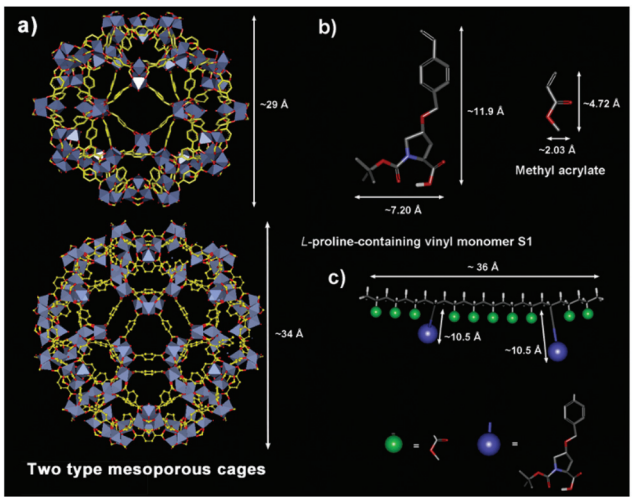

Fig. 2 The topological characteristics of (a) Cr-MIL-101, (b) methyl acrylate and the L-proline-containing vinyl derivative (S1), and (c) the proposed model for the encapsulated linear polymer PP-1-Boc (two repetitive units).

in Fig. 1; the L-proline moieties were adequately intertwined with the MOF architecture by a sufficient number of methyl acrylate groups as copolymerization units. Due to the nature of linear, relatively short, and isolated polymeric chains within the MOF, the dissolution/swelling process of L-proline-containing polymers would be facile because of the minimized polymer–polymer interaction. The dissolution of the chiral polymeric chains **PP1**, which were extracted from **MIL-101-PP1**, is significantly easier than that of the typically used L-proline-containing cross-linked **CPP1** resin (see the ESI for details, Fig. S2†). For a catalyst to be of interest, all catalytic sites within the composites should be sufficiently exposed to the reaction substrates in such a locally homogeneous domain. Besides, the completely solvated polymers can be spatially trapped within the MOF framework, and the leaching of the polymers would not be allowed during catalysis. The facile separation of the composites from the reaction mixtures can be achieved, resulting in their green/sustainable features. Thus, the structures of the synthesized MOF/chiral polymer composites are considerably different from those of homochiral MOFs[12–28] and the conventional functionalized cross-linked polyethylene resins,[59] both of which are pure heterogeneous materials.

Morphological characterization of MIL-101-PP1

Scanning electron microscopy (SEM) and transmission electron microscopy (TEM) images revealed the predominant polymerization of vinyl monomers inside the **Cr-MIL-101** mesopores without the bulk polymer on the external surface (Fig. 3b and Fig. S3†). In addition, the powder X-ray diffraction (PXRD) patterns of both composites were similar to that of **Cr-MIL-101**, confirming the retention of the parent framework structure with octahedron-like morphology. The intensity decreased in the small angle range (2θ, 5–7°), which generally corresponded to the local electron density distortion of the MIL-101 crystal structure upon pore filling (Fig. 4d). The gas

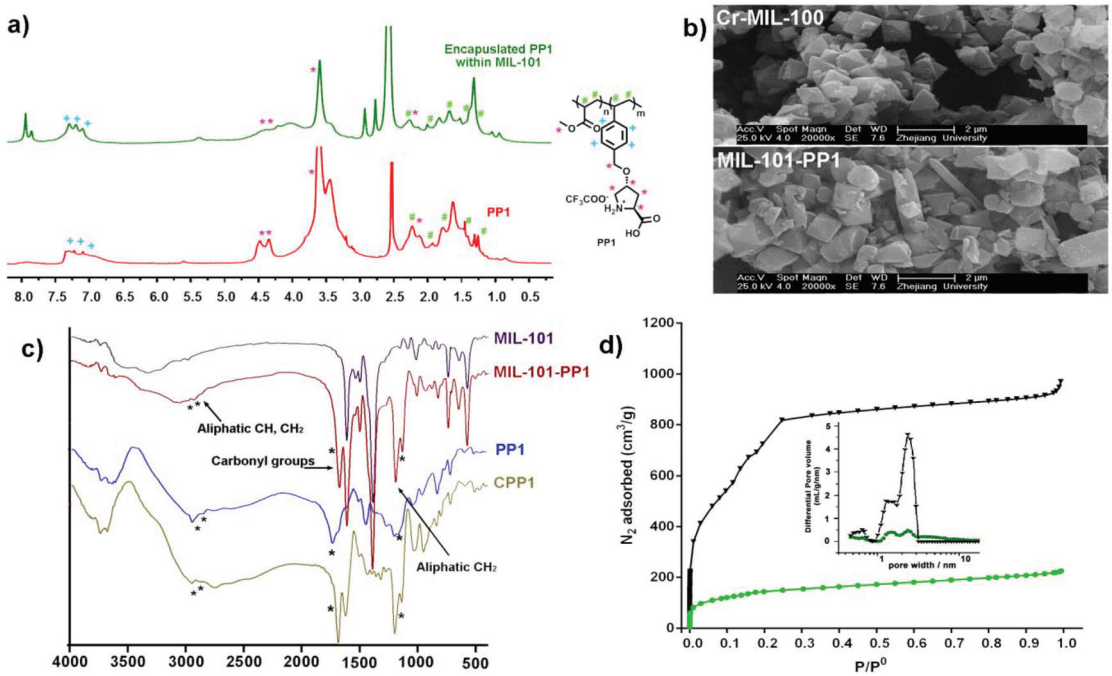

Fig. 3 (a) ^{1}H-NMR spectra of encapsulated polymers of the digested **MIL-101-PP1** (DMSO-d_6) and the bulk **PP1** (MeOH-d_4) prepared using a solution approach. (b) SEM images of **Cr-MIL-101** and **MIL-101-PP1**. (c) IR spectra of **Cr-MIL-101**, **PP1**, **MIL-101-PP1** and **CPP1**. (d) N_2 isotherms and pore-size distribution for **Cr-MIL-101** (black) and **MIL-101-PP1** (green).

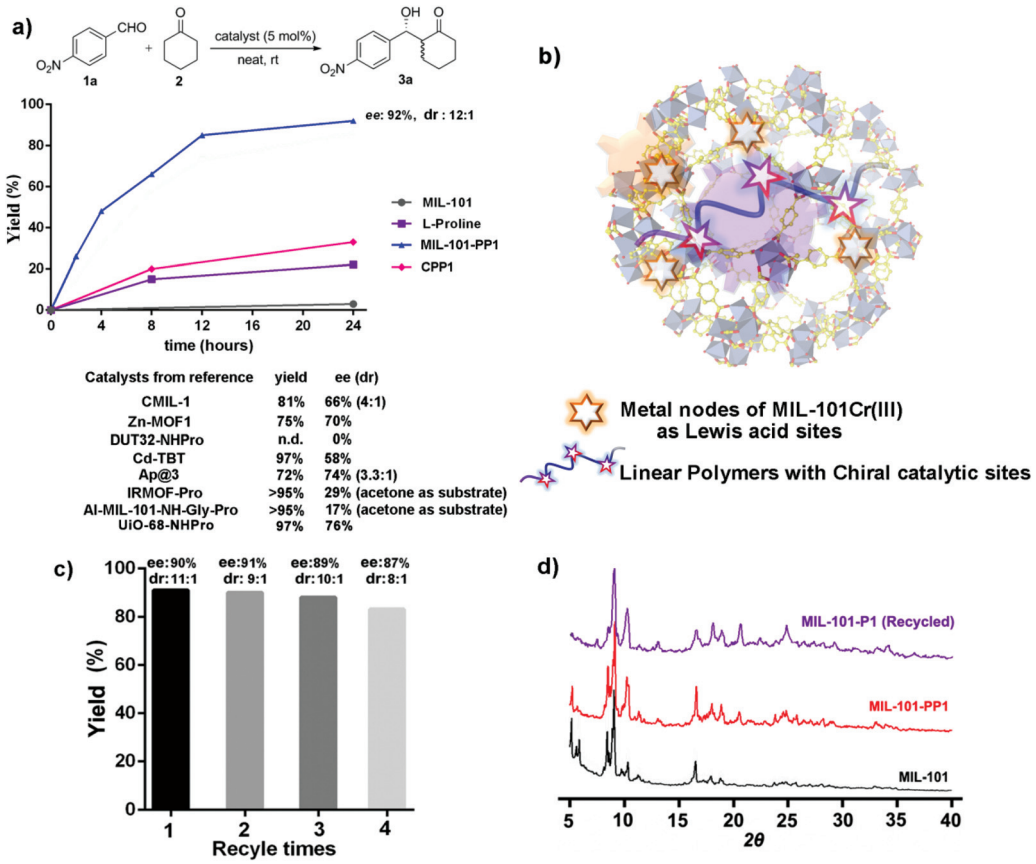

Fig. 4 (a) The contrasting catalytic performance of **MIL-101-PP1**, L-proline, **Cr-MIL-101** and **CPP1**; all of the reactions were performed for 24 h and the yields were determined by ^{1}H NMR spectroscopy using dibromomethane as an internal standard. The ee values were determined by chiral HPLC. The dr values (*anti* : *syn*) were determined by the ^{1}H NMR analysis of the crude reaction mixtures. (b) Schematic diagram for the cooperative effect of **MIL-101-PP1**; (c) the recyclable catalytic ability of **MIL-101-PP1** in the asymmetric Aldol reaction. (d) PXRD measurements of **Cr-MIL-101**, and freshly prepared and 4th recycled **MIL-101-PP1**.

adsorption behaviours of these MOFs (Fig. 3d) revealed that the chiral polymer/MOF composites **MIL-101-PP1** still exhibit high porosity (BET surface area of **MIL-101-PP1:** 531.2 m^{-2} g^{-1}). Neat **Cr-MIL-101** exhibited a type-I N_2 isotherm with stepwise N_2 uptake in the range of 0.1–0.2 p/p°, while **PP1** encapsulated within **Cr-MIL-101** exhibited a relatively smooth N_2 isotherm, indicative of a higher amount of a heterogeneous internal surface because of the incorporated polymer.[60] The calculated Brunauer–Emmett–Teller (BET) surface area decreased from 2980.2 m^2 g^{-1} (pore volume = 1.81 mL g^{-1}) for **Cr-MIL-101** to 531.2 m^2 g^{-1} (pore volume = 0.33 mL g^{-1}) for **MIL-101-PP1**. Such a drastic decrease in the surface area is related to the mass fraction increase of **Cr-MIL-101** and immobilized polymers; thus, the introduced **PP1** must be present inside the cavities of **Cr-MIL-101**. Nevertheless, the pore volume (0.33 mL g^{-1}) of **MIL-101-PP1** would still provide sufficient guest-accessible room for catalysis.

Characterization of internal polymers intertwined into Cr-MIL-101

The linear polymer **PP1** intertwined into the **MIL-101-PP1** cavities was released and collected by the digestion of **Cr-MIL-101** under basic conditions (see the ESI† for details). The released polymers were characterized by ^{1}H NMR spectroscopy (Fig. 3a). Overall, the proton chemical shifts and integral area were consistent with those of **PP1**, which was prepared under homogeneous conditions without **Cr-MIL-101** (see the ESI† for details). More specifically, the broad peaks ranging from 4 to 4.5 ppm corresponded to the heteroatom-attaching aliphatic H of L-proline and benzyl hydrogen protons, while the broad peaks between 6.5 and 7.4 ppm corresponded to the aromatic H of L-proline, demonstrating the successful anchorage of L-proline during *in situ* copolymerization. Meanwhile, the FTIR spectra of **MIL-101-PP1** revealed two new peaks at ~3000 and ~1220 cm^{-1} and ~1700 cm^{-1}, corresponding to the alkyl and carbonyl groups of L-proline/methyl acrylate, respectively (Fig. 3c); these peaks were also observed in the spectra of **PP1** prepared under homogeneous conditions without **Cr-MIL-101** (see the ESI† for details). Thus, the comparison of the FTIR spectrum of neat **Cr-MIL-101** provides additional evidence for the immobilization of L-proline and polymerization of the alkyl moiety into the cavities of **Cr-MIL-101**. Moreover, according to the proton spectral analysis of the released polymer **PP1** with the addition of an internal standard (*i.e.*, trimesic acid),

the molar ratio of the L-proline moiety attaching the polymers to trimesic acid can be calculated by the comparison of the integral areas of the characteristic peaks of 4-benzyloxy-L-proline (broad peak, δ, ranging from 6.5 to 7.4 ppm) and trimesic acid (single peak, δ, 8.37 ppm), affording the catalyst loading amount (related to the proline amount in the material) of the prepared composites **MIL-101-PP1** (eqn (1)). Next, the *in situ* polymerization of impregnated chiral monomers within **Cr-MIL-101** was extensively carried out to investigate the effect of the amount of methyl acrylate (copolymeric vinyl monomers, 5, 10, and 20 equiv.) in *in situ* polymerization; to our delight, the promising catalyst loading amount (L-proline moiety loading, 0.28 mmol per g of the composites, Table 1) was achieved using a 1 : 5 molar ratio of the L-proline-containing vinyl derivative S1 to methyl acrylate (5 equiv.) for polymerization. With the dilution of the concentration of catalytic sites, the catalyst loading amount (L-proline moiety) dramatically decreased, *i.e.*, 0.05 mmol L-proline moiety per gram of the composites (methyl acrylate, 10 equiv.) and <0.01 mmol L-proline moiety per gram of the composites (methyl acrylate, 20 equiv.) (Table S1, characterization can be seen in Fig. S4, Table S2†). This dramatic decrease in the loading amount is related to the remarkably increased flexibility of the linear polymers with an additional number of copolymer units (the size is considerably smaller) that can be easily washed out during the workup. In addition to the NMR analysis, the thermogravimetric analysis (TGA, Fig. S5†) of **MIL-101-PP1** (L-proline moiety loading, 0.28 mmol per g of the composites) revealed an additional weight loss compared to that of **Cr-MIL-101**, corresponding to the thermal decomposition of encapsulated **PP1**. Compared to the weight and molar content of **PP1** within **Cr-MIL-101**, the ratio of the polymerized L-proline-containing vinyl derivative S1 and copolymer methyl acrylate in one polymerization unit was ~8 : 1 for **MIL-101-PP1**. Furthermore, the molecular weight of the released **PP1-Boc** polymer as characterized by gel permeation chromatography was M_w ~ 7374 for **PP1-Boc** (Fig. S6†). This molecular weight is equivalent to *ca.* eight polymerization units of **PP1-Boc**, the length of which is sufficient to intertwine into different cavities of **Cr-MIL-101**.

Table 1 Textural structure and amount of the active site of the catalytic composites

Sample	BET surface area ($m^3\ g^{-1}$)	Pore volume (mL g^{-1})	Amount of the active site (mmol g^{-1})
Cr-MIL-101	2980.2	1.81	0
MIL-101-PP1	531.2	0.33	0.28[a]
PP1	—	—	1.41[a]
CPP1	17.9	0.015	1.55[b]

[a] Active site is defined as L-proline groups on the polymer and the amount is determined based on the loadings of the polymer in the composites (eqn (1)). [b] The amount is determined based on elemental analysis.

Catalytic performance of MIL-101-PP1 in a symmetric Aldol reaction

After the chiral polymer/MOF composites were prepared, they were applied as heterogeneous catalysts in the asymmetric direct Aldol reaction. To our delight, **MIL-101-PP1** with a loading of 5 mol% (related to the proline amount in the material) efficiently catalyzed this reaction, affording **3a** in 91% yield with excellent diastereoselectivity (*anti* : *syn* = 12 : 1) and enantioselectivity (92% ee) (Fig. 4a), with turn-over frequency (TOF) and turn-over number (TON) values of 0.76 h^{-1} and 18.2, respectively. Furthermore, we found that there is no further elimination by-product (crotonization reaction) in our catalysis, by comparing with a control compound (Fig. S7†).[61] In contrast, an extremely low yield (20%) and poor diastereoselectivity (1.1 : 1) were achieved using 5 mol% of L-proline as the homogeneous catalyst under otherwise identical reaction conditions. Besides, the use of 5 mol% (related to the proline amount in the material) of the conventional L-proline-containing cross-linked polystyrene resin **CPP1** (BET surface: 17.9 $cm^2\ g^{-1}$; pore volume: 0.015 mL g^{-1}, see the ESI† for details) afforded the desired product in 33% yield with poor diastereoselectivity (3 : 1 dr) and enantioselectivity (41% ee).

Furthermore, the catalytic ability of the simple physical mixture of **Cr-MIL-101/CPP1** and **Cr-MIL-101/PP1** for the Aldol reaction was not as good as that of **MIL-101-PP1**, only affording the desired product with yields of 35% (5.6 : 1 dr, 84% ee) and 64% (4.5 : 1 dr, 76% ee). By relating the catalytic ability from these contrasting experiments to their structural characteristics and the results from other L-proline-bearing homochiral MOF catalysts (*i.e.*, CMIL-1,[13] Cd-TBT,[20] Zn-MOF1,[21] Ap@3,[23] Al-MIL-101-NH-Gly-Pro,[28] IRMOF-Pro,[62] DUT-32-NHPro,[63] and UiO-68-NHPro,[64] Fig. 4a), the synergistic effect of high porosity and Lewis acidity of **Cr-MIL-101** is thought to be beneficial to the catalytic ability of L-proline in the asymmetric Aldol reaction, which would be attributed to more opportunity to have a cooperative effect between linear polymers threading within MOFs and their nearby catalytic metal nodes (Fig. 4b). Besides, the importance of metal clusters was demonstrated by a control experiment; we blocked the chromium sites of MIL-101-PP1 with pyridine coordination,[13,65] and found that the catalytic ability of **pyridine-grafted MIL-101-PP1** for the Aldol reaction was significantly decreased, only affording the desired product **3a** in 42% yield (3.1 : 1 dr, 58% ee).

Then, the filtration experiment was performed; a suspension of *p*-nitrobenzaldehyde (0.1 mmol), cyclohexanone (0.1 mL) and **MIL-101-PP1** (5 mol%, related to the proline amount in the material) was stirred for 4 hours, and then, **MIL-101-PP1** was filtered off and the filtrate was stirred for another 20 hours. We found that the conversion of the reaction was stopped in the absence of **MIL-101-PP1**, with only 52% yield. We also analyzed the catalyst loading amount of the **recovered MIL-101-PP1** from the catalysis (run once); the active sites (related to the proline amount in the material, 0.23 mmol per g of the composites, Table S2†) in the composites can be

maintained. Therefore, the compact intertwining state of linear chiral polymers and the MOF architecture renders them as robust heterogeneous materials. Furthermore, with the aim to demonstrate the greenness and sustainable profile of **MIL-101-PP1**, it was isolated and reused; the yield of the 5th run was about 91% of the value of the 1st run (Fig. 4c). Furthermore, compared with the PXRD peaks of MIL-101-PP1 and MIL-101-PP1 (recycled) (Fig. 4d), the peak patterns of both the composites were similar, confirming the retention of the parent framework structure with octahedron-like morphology. The slight widening of the peaks and the weakened intensity of low angle peaks (5–9°) can also be observed in the PXRD of **MIL-101-PP1**, since the recycled MIL-101-PP1 becomes much thinner during the reaction.

These preliminary results encouraged us to explore the generality of the reaction system by using various aldehydes. A series of aromatic aldehydes bearing electron-withdrawing groups at different positions of the phenyl ring efficiently reacted, affording the expected products **3b–3g** in good-to-excellent yields (63–99%, Table 2) with excellent enantioselectivities for the major isomer (87–96% ee) and good-to-excellent diastereoselectivity (8 : 1 to >20 : 1 dr) (entries 1–6). Next, bulk aldehyde **1h** was examined (entry 7), the size of which is even greater than the window size of **Cr-MIL-101**. However, the desired product was only obtained in trace amount using 5 mol% **MIL-101-PP1** as the catalyst even after 5 days (in contrast, the product was obtained in 81% yield using 20 mol% of L-proline as the catalyst for 24 h under homogeneous conditions), demonstrating that catalysis mainly occurs within the MOF pores; hence, reagent size selectivity is verified for such a heterogeneous catalyst.

Table 2 **MIL-101-PP1**-catalyzed asymmetric Aldol reaction[a]

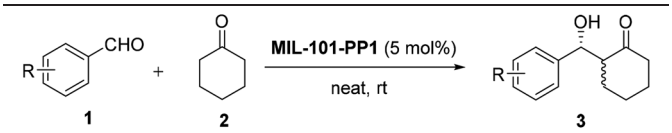

1 2 3

Entry	Aldehyde	3	Time	Yield[b] (%)	ee[c] (%)/dr[d]
1	**1b**: R = *m*-NO_2	**3b**	36 h	86	92 (11 : 1)
2	**1c**: R = *o*-NO_2	**3c**	5 d	87	93 (13 : 1)
3	**1d**: R = *p*-Cl	**3d**	6 d	63	87 (8 : 1)
4	**1e**: R = *p*-CF_3	**3e**	24 h	70	93 (>20 : 1)
5	**1f**: R = *p*-CN	**3f**	48 h	99	91 (8 : 1)
6	**1g**: R = pent-F	**3g**	24 h	89	96 (>20 : 1)
7	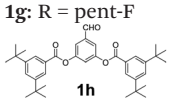	**3h**	5 d	Trace	n.d.

1h

[a] Reactions were carried out under neat conditions using 0.1 mmol aldehyde and 0.1 mL of ketone. [b] The yield was determined by ^{1}H NMR spectroscopy of the crude reaction mixtures using dibromomethane as an internal standard. [c] The ee values were determined by chiral HPLC. [d] dr values (*anti* : *syn*) were determined by the ^{1}H NMR analysis of the crude reaction mixtures; n.d. = not determined.

Conclusion

In this study, highly porous chiral polymer/MOF composites were prepared by a rational design, featuring a strategy involving the *in situ* polymerization of pre-impregnated chiral monomers within MOFs. The chiral catalytic sites attached within the linear polymers were flexible; hence, a synergetic effect between the chiral catalytic sites and Lewis acidic metal nodes is observed for the catalysts. Moreover, the presence of locally homogeneous domains within the globally heterogeneous host rendered benefits of both homogeneous and heterogeneous characteristics to this catalytic system. As expected, excellent diastereo- and enantioselectivities were observed for the asymmetric direct Aldol reaction compared with those observed for heterogeneous and homogeneous catalysis. Therefore, our strategy opens a new perspective for the development of chiral MOFs and other materials as artificial, green and efficient biomimetic systems readily and economically. Currently, studies aimed at extending this strategy to other linear polymers and various applications (*e.g.*, asymmetric catalysis,[10,66] chromatography,[67,68] and sensing[69–71]) are underway in our laboratory.

Experimental section

Chemicals and characterization

NMR spectra were recorded on a Brüker DPX-400/500 spectrometer at 400/500 MHz for ^{1}H NMR and 100/125 MHz for ^{13}C NMR. The data for ^{1}H NMR are recorded as follows: chemical shift (ppm), multiplicity (s, singlet; d, doublet; t, triplet; q, quartet; m, multiplet), coupling constant (Hz), integration. The data for ^{13}C NMR are reported in terms of chemical shift (δ, ppm). Mass spectra were recorded on an Esquire-LC-00075 mass spectrometer. All infrared experiments were performed on a Brüker Alpha FT-IR spectrometer using 1 mg of the solid sample at 4 cm^{-1} resolution. Powder X-ray diffraction (PXRD) data were obtained at ambient temperature on a Bruker D8 Advance diffractometer at 40 kV, 40 mA for Cu Kα (λ = 1.5418 Å), with a scan speed of 1 s per step and a 2θ range of 5–40°. The Brunauer–Emmett–Teller (BET) surface areas were measured by using a Micromeritics ASAP 2020 analyzer at 77 K. Thermogravimetric analysis (TGA) data were obtained using a PerkinElmer TGA 7 system running from 50 °C to 500 °C with a scan rate of 10 °C min^{-1}. The analyses of the morphology and chemical composition of the samples were conducted by using a Hitachi S-4800 field emission scanning electron microscope (FE-SEM). The computational modeling for the topological characteristics of the host, monomers, and linear polymers was achieved by using the Discovery Studio 2.5 program. Gel permeation chromatography (GPC) analysis was performed on a Waters 1525 system with a refractive index (RI) detector. The starting materials and solvents were purchased and used without further purification from commercial suppliers (Sigma-Aldrich, Alfa Aesar, TCI, and others).

The synthesis of MIL-101-PP1 composites

A solution of compound **S1** (300 mg, 0.86 mmol), methyl acrylate (4.3 mmol, as a co-polymeric monomer) and 2,2-azobisisobutyronitrile (AIBN, 42.3 mg, 0.26 mmol, as a radical initiator) in toluene (2 mL) was impregnated into **Cr-MIL-101** (1 g), and the mixture was allowed to stand under a nitrogen atmosphere at 4 °C for 12 hours to reach a distribution equilibrium of the monomers through the cavities of MIL-101. The polymerization was conducted under a nitrogen atmosphere at 80 °C for 5 days. Then, the obtained powder was soaked in DMF for 3 days to completely remove all unreacted monomer and loosely attached polymers between MIL-101 particles. DMF was then removed by washing with CH_2Cl_2. Finally, the desired polymer **MIL-101-PP1** was obtained by further deprotection of the *N*-Boc group in a mixture of CH_2Cl_2 (4 mL) and CF_3CO_2H (1 mL) for 4 hours at room temperature, and was successively washed with CH_2Cl_2 and dried at 80 °C overnight.

The extraction of linear polymers PP1 from MIL-101-PP1 composites

Prior to the deprotection of *N*-Boc, the **MIL-101-PP1** composites (200 mg) were fully digested using 10 wt% sodium hydroxide aqueous solution (0.8 mL); then the mixture was acidified to neutral pH (pH ~ 7) using 6N hydrochloric acid. With the aim to precipitate terephthalic acid and salts (*e.g.* NaCl and $CrCl_3$), acetone (50 mL) was added, and a brownish solution was obtained by filtration. Then, the extracted mixture was concentrated under vacuum to afford **PP1-Boc**. Subsequently, **PP1-Boc** was added to CH_2Cl_2 (4 mL) and CF_3CO_2H (1 mL) and stirred for 4 hours at room temperature to completely remove the *N*-Boc group, and the desired linear polymers **PP1** were obtained by the evaporation of the reaction solvent.

Qualification for the L-proline loading amount with a unit of mmol g^{-1} in the MIL-101-PP1 composite

The **MIL-101-PP1** composite (200 mg) was first fully digested with a mixture of 10 wt% NaOD and MeOH-d_4 (1 : 2, v/v). The filtrate was collected and the internal standard trimesic acid (21 mg, 0.1 mmol) was added (slightly heated to dissolve it); then the ^{1}H-NMR analysis of the mixture was performed. The molecular constitution of the released **PP1** involves an L-proline-containing unit and methyl acrylate units; indeed, NMR analysis can exactly give the value of the **PP1**/trimesic acid molar ratio, which can be calculated by the ratio of the integral areas between the characteristic phenyl peaks of 4-benzyloxy-L-proline (IA_{PP1}, broad peak, δ, ranging from 6.5 to 7.4 ppm) and trimesic acid ($IA_{trimesic\ acid}$, δ, 8.37 ppm). Therefore, the L-proline loading amount with a unit of mmol g^{-1} can be calculated based on eqn (1):

$$\frac{\frac{IA_{PP1}}{IA_{trimesic\ acid}} \times 0.1 \times \frac{3}{4} \times W_{PP1}}{W_{PP1}} \times \frac{1000}{200} \quad (1)$$

Typical reaction procedure for the Aldol reaction

A suspension of the aldehyde (0.1 mmol) and cyclohexanone (0.1 mL) and the corresponding chiral catalyst (0.005 mmol, 17.8 mg for **MIL-101-PP1**) was stirred at room temperature for the indicated time (Table 2). The reaction was quenched by adding ethyl acetate. Upon filtration, the catalyst was washed with CH_2Cl_2. The organic layers were collected and concentrated under vacuum. The crude product was checked by ^{1}H NMR spectroscopy to obtain the reaction yield and diastereoselectivity (dr values) using dibromomethane as an internal standard, and was then purified by chromatography (petroleum ether/ethyl acetate) to afford the desired product. The ee value was determined by chiral stationary phase HPLC analysis.

Conflicts of interest

There are no conflicts to declare.

Acknowledgements

The authors gratefully acknowledge Prof. Chi-Ming Che of The Hong Kong University for his knowledge sharing and suggestions on the concept of the heterogenization of homogeneous chiral polymers in metal–organic frameworks and its application in asymmetric catalysis.

Financial support from the National Natural Science Foundation of China (No. 21722203, 51603046, and 21572096), the Shenzhen Special Funds (JCYJ20170307105638498) and the Shenzhen Nobel Prize Scientists Laboratory Project (C17213101) is greatly appreciated.

References

1 R. Breslow, *Acc. Chem. Res.*, 1995, **28**, 146.
2 S. J. Benkovic and S. Hammes-Schiffer, *Science*, 2003, **301**, 1196.
3 G. Wulff, *Chem. Rev.*, 2002, **102**, 1.
4 V. Blanco, D. A. Leigh and V. Marcos, Artificial switchable catalysts, *Chem. Soc. Rev.*, 2015, **44**, 5341.
5 J. Shi, *Chem. Rev.*, 2013, **113**, 2139.
6 U. Díaz, D. Brunel and A. Corma, *Chem. Soc. Rev.*, 2013, **42**, 4083.
7 J. A. Mata, F. E. Hahn and E. Peris, *Chem. Sci.*, 2014, **5**, 1723.
8 P. Buchwalter, J. Rosé and P. Braunstein, *Chem. Rev.*, 2015, **115**, 28.
9 Y. Liu, W. Xuan and Y. Cui, *Adv. Mater.*, 2010, **22**, 4112.
10 M. Yoon, R. Srirambalaji and K. Kim, *Chem. Rev.*, 2012, **112**, 1196.
11 L. Ma, C. Abney and W. Lin, *Chem. Soc. Rev.*, 2009, **38**, 1248.

12 J. S. Seo, D. Whang, H. Lee, S. I. Jun, J. Oh, Y. J. Jeon and K. A. Kim, *Nature*, 2000, **404**, 982.
13 M. Banerjee, S. Das, M. Yoon, H. J. Choi, M. H. Hyun, S. M. Park, G. Seo and K. Kim, *J. Am. Chem. Soc.*, 2009, **131**, 7524.
14 O. R. Evans, H. L. Ngo and W. Lin, *J. Am. Chem. Soc.*, 2001, **123**, 10395.
15 L. Ma, J. M. Falkowski, C. Abney and W. Lin, *Nat. Chem.*, 2010, **2**, 838–846.
16 C. D. Wu, A. Hu, L. Zhang and W. Lin, *J. Am. Chem. Soc.*, 2005, **127**, 8940.
17 J. M. Falkowski, T. Sawano, T. Zhang, G. Tsun, Y. Chen, J. V. Lockard and W. Lin, *J. Am. Chem. Soc.*, 2014, **136**, 5213.
18 Q. Han, C. He, M. Zhao, B. Qi, J. Niu and C. Duan, *J. Am. Chem. Soc.*, 2013, **135**, 10186.
19 P. Wu, C. He, J. Wang, X. Peng, X. Li, Y. An and C. Duan, *J. Am. Chem. Soc.*, 2012, **134**, 14991.
20 D. Dang, P. Wu, C. He, Z. Xie and C. Duan, *J. Am. Chem. Soc.*, 2010, **2**, 14321.
21 W. Zhu, C. He, P. Wu, X. Wu and C. Duan, *Dalton Trans.*, 2012, **41**, 3072.
22 K. Mo, Y. Yang and Y. Cui, *J. Am. Chem. Soc.*, 2014, **136**, 1746.
23 Y. Liu, X. Xi, C. Ye, T. Gong, Z. Yang and Y. Cui, *Angew. Chem., Int. Ed.*, 2014, **53**, 13821.
24 C. Zhu, G. Yuan, X. Chen, Z. Yang and Y. Cui, *J. Am. Chem. Soc.*, 2012, **134**, 8058.
25 D. J. Lun, G. I. Waterhouse and S. G. Telfer, *J. Am. Chem. Soc.*, 2011, **133**, 5806.
26 K. S. Jeong, Y. B. Go, S. M. Shin, S. J. Lee, J. Kim, O. M. Yaghi and N. Jeong, *Chem. Sci.*, 2011, **2**, 877.
27 S. H. Cho, B. Ma, S. T. Nguyen and J. T. Hupp, *Chem. Commun.*, 2006, 2563.
28 J. Bonnefoy, A. Legrand, E. A. Quadrelli, J. Canivet and D. Farrusseng, *J. Am. Chem. Soc.*, 2015, **137**, 9409.
29 K. Manna, P. Ji, F. X. Greene and W. Lin, *J. Am. Chem. Soc.*, 2016, **138**, 7488.
30 K. Manna, P. Ji, Z. Lin, F. X. Greene, A. Urban, N. C. Thacker and W. Lin, *Nat. Commun.*, 2016, **7**, 12610.
31 M. H. Beyzavi, N. A. Vermeulen, A. Howarth, J. S. Tussupbayev, A. B. League, N. M. Schweitzer, J. R. Gallagher, A. E. Platero-Prats, N. Hafezi, A. A. Sarjeant, J. T. Miller, K. W. Chapman, J. F. Stoddart, C. J. Cramer, J. T. Hupp and O. K. Farha, *J. Am. Chem. Soc.*, 2015, **137**, 13624.
32 C. Baleizao, B. Gigante, D. Das, M. Álvaro, H. García and A. Corma, *Chem. Commun.*, 2003, **15**, 1860.
33 P. Agrigento, S. M. Al-Amsyar, B. Sorée, M. Taherimehr, M. Gruttadauria, C. Aprile and P. P. Pescarmona, *Catal. Sci. Technol.*, 2014, **4**, 1598.
34 G. Distefano, H. Suzuki, M. Tsujimoto, S. Isoda, S. Bracco, A. Comotti, P. Sozzani, T. Uemura and S. Kitagawa, *Nat. Chem.*, 2013, **5**, 335.
35 T. Uemura, Y. Ono, Y. Hijikata and S. Kitagawa, *J. Am. Chem. Soc.*, 2010, **132**, 4917.
36 L. Gao, C. Y. Li, K. Y. Chan and Z. N. Chen, *J. Am. Chem. Soc.*, 2014, **136**, 7209.
37 T. Uemura, N. Uchida, A. Asano, A. Saeki, S. Seki, M. Tsujimoto, S. Isoda and S. Kitagawa, *J. Am. Chem. Soc.*, 2012, **134**, 8360.
38 C. R. Mulzer, L. Shen, R. P. Bisbey, J. R. McKone, N. Zhang, H. D. Abruña and W. R. Dichtel, *ACS Cent. Sci.*, 2016, **2**, 667.
39 J. S. Brian, L. R. Parent, A. C. Overholts, P. A. Beaucage, R. P. Bisbey, A. D. Chavez, N. Hwang, C. Park, A. M. Evans, N. C. Gianneschi and W. R. Dichtel, *ACS Cent. Sci.*, 2017, **3**, 58.
40 L. Gao, C. V. Li and K.-Y. Chan, *Chem. Mater.*, 2015, **27**, 3601.
41 Q. Sun, B. Aguila, J. A. Perman, N. T. K. Nguyen and S. Ma, *J. Am. Chem. Soc.*, 2016, **138**, 15790.
42 L. Bai, P. Wang, P. Bose, P. Li, R. Zou and Y. Zhao, *ACS Appl. Mater. Interfaces*, 2015, **7**, 5056.
43 J. S. Lin, F. L. Wang, X. Y. Dong, W. W. He, Y. Yuan, S. Chen and X. Y. Liu, *Nat. Commun.*, 2017, **8**, 14841.
44 J. S. Lin, X. Y. Dong, T. T. Li, N. C. Jiang, B. Tan and X. Y. Liu, *J. Am. Chem. Soc.*, 2016, **138**, 9357.
45 J. S. Lin, P. Yu, L. Huang, B. Tan and X.-Y. Liu, *Angew. Chem., Int. Ed.*, 2015, **54**, 7847.
46 X. W. Dong, T. Liu, Y. Z. Hu, X. Y. Liu and C. M. Che, *Chem. Commun.*, 2013, **49**, 7681.
47 T. Liu, J. X. Che, Y. Z. Hu, X. W. Dong, X. Y. Liu and C. M. Che, *Chem. – Eur. J.*, 2014, **20**, 14090.
48 T. Liu, D. Q. Li, S. Y. Wang, Y. Z. Hu, X. W. Dong, X. Y. Liu and C. M. Che, *Chem. Commun.*, 2014, **50**, 13261.
49 F. M. Zhang, S. Zheng, Q. Xiao, Y. J. Zhong, W. D. Zhu, A. Lin and M. S. El-Shall, *Green Chem.*, 2016, **18**, 2900–2908.
50 J. L. Song, Z. F. Zhang, S. Q. Hu, T. B. Wu, T. Jiang and B. X. Han, *Green Chem.*, 2009, **11**, 1031–1036.
51 C. Parmeggiani, C. Matassini and F. Cardona, *Green Chem.*, 2017, **19**, 2030–2050.
52 A. Dhakshinamoorthy, A. M. Asiri, M. Alvaro and H. Garcia, *Green Chem.*, 2018, **20**, 86–107.
53 M. Penhoat, D. Barbry and C. Rolando, *Tetrahedron Lett.*, 2011, **52**, 159.
54 B. List, *Tetrahedron*, 2002, **58**, 5573.
55 G. Ferey, C. Mellot-Draznieks, C. Serre, F. Millange, J. Dutour, S. Surble and I. Margiolaki, *Science*, 2005, **309**, 2040.
56 O. V. Zalomaeva, A. M. Chibiryaev, K. A. Kovalenko, O. A. Kholdeeva, B. S. Balzhinimaev and V. P. Fedin, *J. Catal.*, 2013, **298**, 179.
57 B. List, R. A. Lerner and C. F. Barbas III, *J. Am. Chem. Soc.*, 2000, **122**, 2395.
58 A. B. Northrup, I. K. Mangion, F. Hettche and D. W. C. MacMillan, *Angew. Chem., Int. Ed.*, 2004, **43**, 2152.
59 J. Lu and P. H. Toy, *Chem. Rev.*, 2009, **109**, 815.
60 M. Choi, F. Kleitz, D. Liu, H. Y. Lee, W. S. Ahn and R. Ryoo, *J. Am. Chem. Soc.*, 2005, **127**, 1924.
61 G. V. Austerweil and R. Pallaud, *J. Appl. Chem.*, 1955, **5**, 213.

62 L. Liu, X. Zhang, S. Rang, Y. Yang, X. Dai, J. S. Gao, C. Xu and J. He, *RSC Adv.*, 2014, **4**, 13093.
63 C. Kutzscher, H. C. Hoffmann, S. Krause, U. Stoeck, I. Senkovska, E. Brunner and S. Kaskel, *Inorg. Chem.*, 2015, **54**, 1003.
64 C. Kutzscher, G. Nickerl, I. Senkovska, V. Bon and S. Kaskel, *Chem. Mater.*, 2016, **28**, 2573.
65 F. Yang, C.-X. Yang and X.-P. Yan, *Talanta*, 2015, **137**, 136.
66 A. H. Chughtai, N. Ahmad, H. A. Younus, A. Laypkovc and F. Verpoort, *Chem. Soc. Rev.*, 2015, **44**, 6804.
67 X. Kuang, Y. Ma, H. Su, J. Zhang, Y. B. Dong and B. Tang, *Anal. Chem.*, 2014, **86**, 1277.
68 S. M. Xie, Z. J. Zhang, Z. Y. Wang and L. M. Yuan, *J. Am. Chem. Soc.*, 2011, **133**, 11892.
69 M. M. Wanderley, C. Wang, C.-D. Wu and W. Lin, *J. Am. Chem. Soc.*, 2012, **134**, 9050.
70 L. Qin, M. X. Zheng, Z. J. Guo, H. G. Zheng and Y. Xu, *Chem. Commun.*, 2015, **51**, 2447.
71 L. H. Cao, Y. L. Wei, C. Ji, M. L. Ma, S. Q. Zang and T. C. W. Mak, *Chem. – Asian J.*, 2014, **9**, 3094.